Kinetic evidence against partitioning of the ubiquinone pool and the catalytic relevance of respiratory-chain supercomplexes

James N. Blaza, Riccardo Serreli, Andrew J. Y. Jones, Khairunnisa Mohammed, and Judy Hirst[1]

Medical Research Council Mitochondrial Biology Unit, Cambridge CB2 0XY, United Kingdom

Edited by Gottfried Schatz, University of Basel, Reinach, Switzerland, and approved September 26, 2014 (received for review July 24, 2014)

In mitochondria, four respiratory-chain complexes drive oxidative phosphorylation by sustaining a proton-motive force across the inner membrane that is used to synthesize ATP. The question of how the densely packed proteins of the inner membrane are organized to optimize structure and function has returned to prominence with the characterization of respiratory-chain supercomplexes. Supercomplexes are increasingly accepted structural entities, but their functional and catalytic advantages are disputed. Notably, substrate "channeling" between the enzymes in supercomplexes has been proposed to confer a kinetic advantage, relative to the rate provided by a freely accessible, common substrate pool. Here, we focus on the mitochondrial ubiquinone/ubiquinol pool. We formulate and test three conceptually simple predictions of the behavior of the mammalian respiratory chain that depend on whether channeling in supercomplexes is kinetically important, and on whether the ubiquinone pool is partitioned between pathways. Our spectroscopic and kinetic experiments demonstrate how the metabolic pathways for NADH and succinate oxidation communicate and catalyze via a single, universally accessible ubiquinone/ubiquinol pool that is not partitioned or channeled. We reevaluate the major piece of contrary evidence from flux control analysis and find that the conclusion of substrate channeling arises from the particular behavior of a single inhibitor; we explain why different inhibitors behave differently and show that a robust flux control analysis provides no evidence for channeling. Finally, we discuss how the formation of respiratory-chain supercomplexes may confer alternative advantages on energy-converting membranes.

supercomplex | respirasome | mitochondria | respiratory chain | ubiquinone

Contemporary models for the organization of respiratory-chain complexes in energy-transducing membranes range from the fluid model to the respirasome model. In the fluid model each complex is a free and independent entity, and substrates exchange freely between enzymes through common ubiquinone/ubiquinol (Q) and cytochrome c_{ox}/c_{red} (cyt c) pools (1–3). In the respirasome model the complexes are assembled into units that contain everything required for catalysis; substrates are channeled between enzymes within the respirasome, not exchanged with external pools (4, 5). Intermediate models, in which some enzymes are free and some assembled into multienzyme supercomplexes, or in which supercomplexes are assembled and disassembled in response to changing conditions, are increasingly considered a realistic combination of these two extremes (6).

Structural evidence for respiratory-chain supercomplexes, initiated by observations by blue native PAGE analyses of mammalian mitochondria (4, 7), has culminated in electron microscopy data that revealed the arrangement of complexes I, III, and IV in a particular class of isolated supercomplex assembly (8, 9); respiratory-chain supercomplexes have also been observed (at lower resolution) in the membrane (10). Furthermore, specific proteins have been found to mediate interactions between specific pairs of respiratory complexes, and functionally removing these proteins prevents the relevant supercomplexes from forming (11–14). Thus, structural associations between membrane-bound respiratory complexes are increasingly accepted.

Whether a catalytic or functional justification for the formation of respiratory-chain supercomplexes exists is uncertain. The most widely cited evidence for a catalytic role, from flux control analysis (15), was considered to support substrate channeling between enzymes present within respirasomes. More recently, the existence of dedicated Q and cyt c pools within supercomplex assemblies was proposed to determine electron transport chain flux, based on the relative rates of complex I- and complex II-linked respiration observed when complexes I and/or III are ablated (13). Opposing these substrate channeling models, a recent time-resolved kinetic study of the respiratory chain in intact yeast cells concluded that cyt c is not trapped within supercomplexes and encounters no restriction to its diffusion (16).

Here, we focus on the mitochondrial Q pool. We formulate and test a set of conceptually simple predictions of the behavior of the mammalian respiratory chain that depend on whether Q channeling in supercomplexes is kinetically important, and on whether the Q pool is partitioned into supercomplex assemblies. Our results are not consistent with Q channeling or partitioning. Consequently, we reevaluate the contrary evidence from flux control analysis and find that the substrate channeling proposal arose from lack of consideration of the effects of enzyme substrate and inhibitor binding properties. We conclude that Q exists as a single, common pool in mammalian mitochondria that is exchanged freely between complexes.

Results

Confirmation of the Presence of Supercomplexes in Submitochondrial Particles and Membrane Preparations. We chose submitochondrial particles (SMPs) and membrane preparations from *Bos taurus*

Significance

Mitochondria produce ATP by using respiration to drive ATP synthase. Respiration is catalyzed by several membrane-bound complexes that are structurally organized into supercomplex assemblies. Supercomplexes have been proposed to confer a catalytic advantage by channeling of substrates between enzymes in the assemblies. Here, we test three simple predictions of the behavior of the mammalian respiratory chain that depend on whether channeling in supercomplexes is kinetically important and show that it is not. We reinterpret previous data taken to support substrate channeling and reveal an alternative explanation for these data. Finally, we discuss alternative proposals for why the respiratory-chain complexes have evolved to form supercomplex structures.

Author contributions: J.N.B., R.S., A.J.Y.J., and J.H. designed research; J.N.B., R.S., A.J.Y.J., and K.M. performed research; J.N.B., R.S., A.J.Y.J., K.M., and J.H. analyzed data; and J.N.B. and J.H. wrote the paper.

The authors declare no conflict of interest.

This article is a PNAS Direct Submission.

[1]To whom correspondence should be addressed. Email: jh@mrc-mbu.cam.ac.uk.

This article contains supporting information online at www.pnas.org/lookup/suppl/doi:10.1073/pnas.1413855111/-/DCSupplemental.

(bovine) heart mitochondria as experimental systems (see *SI Text* for details). SMPs are tightly coupled, inverted vesicles of the inner mitochondrial membrane (17); they were prepared either with or without additional cyt *c*. In SMPs the active sites of complexes I and II are exposed to the external solution (rather than locked inside the mitochondrion), allowing precise control over substrate concentrations and active-site conditions. Membrane preparations have a similar protein composition but they contain membrane fragments rather than sealed vesicles; they are unable to sustain a proton-motive force (Δp), and the active sites of all of the complexes are accessible. Fig. 1 compares blue native PAGE analyses (18) of the bovine heart mitochondria, membranes, and SMP preparations used here, revealing that each preparation contains an equivalent complement of supercomplexes. In-gel activity assays confirmed the presence of complex I (as well as complexes III and IV), but not complex II, in the bands attributed to supercomplexes, consistent with previous reports (4, 7, 13). Thus, SMPs and membranes are appropriate systems for investigating the functional relevance of supercomplexes.

Transfer of Ubiquinol from Complexes I and II to Complex III. It has been proposed that the Q pool is partitioned such that the ubiquinol produced by complex I is channeled to complex III within supercomplex assemblies, whereas the ubiquinol produced by complex II diffuses into the membrane to access a separate complex III population (13, 15). If this is the case, then adding either NADH or succinate to mitochondrial membranes or SMPs should reduce only part of the complex III population, whereas adding both simultaneously should reduce the whole population. If the Q pool is not partitioned into two (a single pool is accessible to all enzymes), then adding NADH or succinate alone should reduce the whole population directly. Here, we monitored the redox status of complex III in SMPs by using a diode-array spectrometer to record spectra between 490 and 650 nm and the classical least squares method in matrix form (with known reference spectra) to deconvolute the difference spectra (i.e., the spectrum of interest minus the starting spectrum) into the contributions of the individual heme centers (19, 20). SMPs were chosen for this experiment because membrane solutions with high enough concentrations for heme spectroscopy are more turbid, resulting in increased light scattering. As an example, Fig. 2*A* shows how the difference spectrum evolves upon addition of succinate to oxidized SMPs, Fig. 2 *B* and *C* present the deconvolution of a single difference spectrum into its individual components, and Fig. 2*D* reveals how the individual complex III heme species vary through the experiment.

Fig. 3 shows how the heme centers in complex III and cyt *c* become reduced upon addition of NADH, or succinate, or both NADH and succinate, to SMPs, in the absence of O_2 to prevent flux, and in the presence of gramicidin to dissipate Δp. The reduction potential of heme c_1 [0.24 V (21)] is considerably higher than that of ubiquinone, so it can essentially be completely reduced by the reduced Q pool. Fig. 3*A* shows that all three reductant combinations (NADH, succinate, and both together) reduce heme c_1 rapidly and to the same extent, so all three of them access all of the complex III present. Heme c_1 transfers electrons to cyt *c*, with a similarly high reduction potential, and Fig. 3*B* shows that each reductant combination also accesses the whole cyt *c* pool. It has been recently argued that the cyt *c* pool is also compartmentalized, like the Q pool (13), but the data in Fig. 3*B* are clear evidence against this proposal.

Using the extinction coefficients of the heme centers (Table S1) revealed that SMPs prepared with additional cyt *c* (see *SI Text* for details) typically contain more than twice as much cyt *c* as complex III, raising the possibility of an artifact whereby a single cyt *c* pool equilibrates two populations of complex III, making two Q pools appear as one. Fig. S1 shows data equivalent to the data in Fig. 3, but from SMPs prepared without additional cyt *c*. Except for the decreased cyt *c* signal the data are indistinguishable, as highlighted by the direct comparison of heme c_1 data (Fig. S2). This comparison excludes the cyt *c* equilibration hypothesis. Finally, Fig. 3 *C* and *D* show that the *b*-hemes in complex III are reduced less completely than heme c_1 (~70% reduction); the reduction is less in succinate and NADH separately than in the presence of both substrates, but, importantly, the difference is far from the additive intensities that would be expected from two separate pools. The incomplete reduction probably reflects the lower reduction potentials of the *b*-hemes [80 mV for b_H and −50 mV for b_L (21)]. In conclusion, the data in Fig. 3 are strong evidence against the partitioning of complex III and therefore the Q pool.

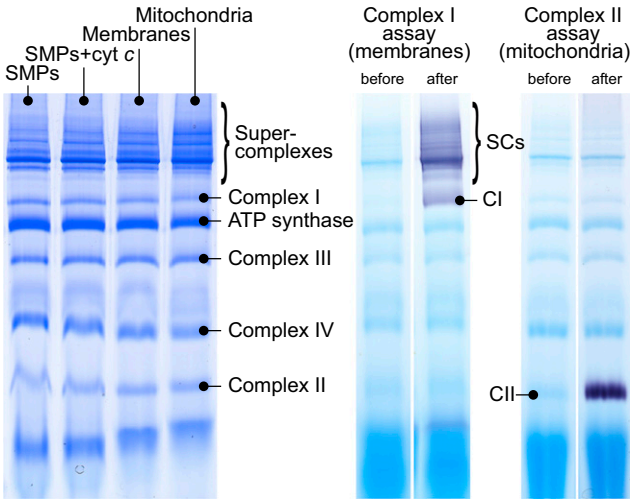

Fig. 1. Blue native PAGE analyses of the supercomplexes present in bovine heart mitochondria, membranes, and SMPs. (*Left*) Coomassie-stained gel showing that SMPs (prepared either with or without additional cyt *c*), membranes, and mitochondria all contain equivalent complements of supercomplexes. (*Middle*) Typical in-gel complex I activity assay (before and after incubation with NADH and NBT) showing the presence of complex I in supercomplexes. (*Right*) Typical in-gel complex II activity assay (before and after incubation with succinate, PMS, and NBT).

Fluxes Through the NADH:O_2 and Succinate:O_2 Pathways Affect Each Other. If complex I and II face two separate Q pools, each linked to its own complex III population, then the fluxes through the NADH:O_2 and succinate:O_2 pathways should be independent of one other (when Δp = 0), because they do not communicate by competing for the same substrate. It is important to collapse Δp to zero because Δp created by one pathway would influence the other, providing an alternative method of communication. Fig. 4 shows the effects of operating both pathways at the same time, with the rates of succinate oxidation altered by inhibition of complex II (by malonate). Four systems were explored: SMPs prepared with and without additional cyt *c* and membranes in the presence or absence of additional cyt *c* (see *SI Text* for details). Lower levels of cyt *c* render the complex III+IV segment of the chain more rate-limiting. Fig. 4 shows that, in every case, the sum of the rates of the NADH:O_2 and succinate:O_2 pathways operating independently is much greater than the rate observed when both pathways operate together. The addition of malonate shows that the effect is reversible. The mutual inhibition is greatest when the cyt *c* level is low, in either SMPs or membranes, because low cyt *c* limits the rate of the complex III+IV segment of the chain that is common to both pathways, capping the total combined flux and making it less dependent on the Q-dependent reactions. Thus, Fig. 4 demonstrates mutual inhibition between the NADH:O_2 and succinate:O_2 pathways, showing that they compete for a common substrate pool.

Rates of Electron Flux Between Complexes I and II Through a Shared Q Pool. Slow exchange between two separate Q pools (relative to the catalytic timescale) would preclude "cross-reactions" (that

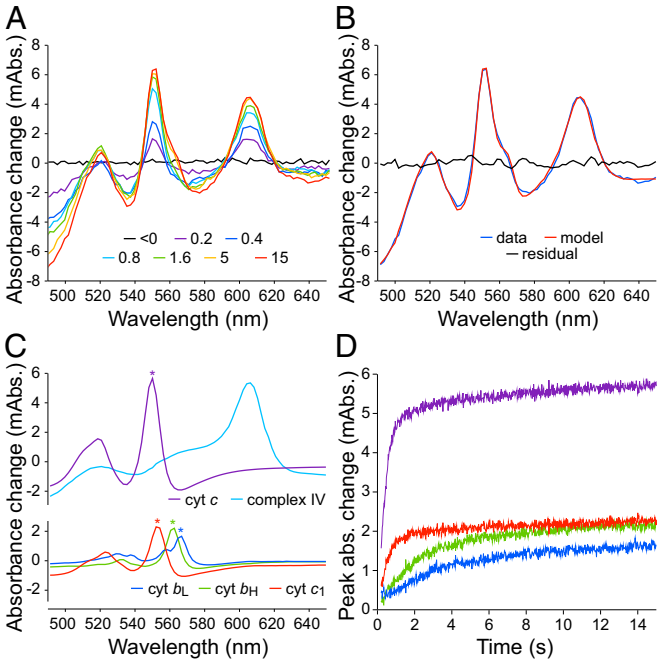

Fig. 2. Spectral analysis of the redox status of the heme centers in complex III. (*A*) Individual difference spectra (relative to the starting spectrum) recorded following the addition of 5 mM succinate to 500 μg·mL^{-1} SMPs in the presence of 5 μg·mL^{-1} gramicidin; the SMPs were prepared with additional cyt *c*. The spectra are shown at the time points indicated (values are in seconds). (*B*) The fit between the difference spectrum recorded at 15 s and the modeled spectrum, calculated as a sum of the individual difference spectra shown in *C* and generated using the classical least squares method in matrix form. (*C*) Spectral components of the b_H, b_L, and c_1 hemes in complex III, cyt c, and complex IV from the model shown in *B* (the spectra of hemes *a* and a_3 in complex IV are combined and the background scatter omitted for simplicity). (*D*) Change in the peak difference absorbances (marked with asterisks in *C*) for the b_H, b_L, and c_1 hemes in complex III, and for cyt *c*, following addition of succinate. Conditions: 10 mM Tris-SO_4 (pH 7.5), 250 mM sucrose, 32 °C.

rely on transfer between the pools) from occurring at significant rates. NADH:fumarate oxidoreduction and succinate:NAD^+ oxidoreduction driven by ATP hydrolysis (reverse electron transfer) are both cross-reactions; Table 1 compares the rate of each reaction discussed here, catalyzed by SMPs. The rate of reverse electron transfer is comparable to the rates of flux through the NADH:O_2 and succinate:O_2 pathways, measured under equivalent conditions; this rapid catalysis cannot rely on slow exchange between two separate Q pools. In contrast, the rate of NADH:fumarate oxidoreduction is relatively low. Although this observation could be viewed as evidence for separate Q pools, it has long been known that the rate of fumarate reduction by complex II is slow; indeed, organisms that use fumarate as a terminal electron acceptor invariably express a different enzyme, fumarate reductase, to catalyze this reaction (22).

Flux Control Analysis. Flux control analysis is the most widely cited evidence for the kinetic relevance of I+III supercomplexes because the flux control coefficients (FCCs) reported for complexes I and III in the NADH:O_2 pathway are both close to 1(15). FCCs denote the contribution of a single enzyme step in controlling the overall flux through a metabolic pathway. An FCC of 1 denotes complete control over the pathway by the individual enzyme (a value of 0 denotes no control) and the FCCs for all of the steps in a pathway must sum to 1 (23). The FCCs for complexes I and III suggested they both exert close to complete control over the pathway flux (15)—this can only be accommodated if they are joined into a single supercomplex that catalyzes a single rate-determining step.

Here, we follow the method used previously (15) to determine the FCCs for complexes I and II within the NADH:O_2 and succinate:O_2 oxidoreduction pathways, respectively. Thus, we compare the effects of inhibitors on the overall flux along the pathways and on the turnover of the individual enzymes; the ratio of inhibitions at low inhibitor concentration (the slopes of the inhibition titration curves as [I] → 0) is the FCC. Fig. S3 shows examples of the inhibitor titrations that were used to determine the FCCs in Table 2. First, we replicated the study of Lenaz and coworkers (15) by testing the effect of rotenone on complex I catalysis (NADH:ubiquinone-1 oxidoreduction) and on NADH:O_2 pathway flux (complexes I+III+IV). Using rotenone, Lenaz and coworkers (15) reported FCCs of 0.91 in SMPs and 1.06 in permeabilized mitochondria, whereas our values range from 1.68 in SMPs to 2.42 in membranes and to 3.86 for membranes in the presence of additional cyt *c* (Table 2). Our rotenone FCCs are all greater than 1, so none of them are meaningful as FCC values. Subsequent investigation of the FCC for complex II (succinate:ubiquinone-1 oxidoreduction) in the succinate:O_2 pathway (complexes II+III+IV) in SMPs using atpenin A5 (24) revealed a similarly meaningless value of 1.17 (Table 2). Using carboxin, an alternative complex II inhibitor, Lenaz and coworkers (15) reported a slightly smaller value, 0.98. We note that complex II was not detected in any of the supercomplexes in Fig. 1, consistent with previous reports (4, 7, 13), so supercomplex formation is not the origin of this behavior. Subsequently, measurements using piericidin A, an alternative complex I inhibitor, revealed that the FCC values observed are dictated by the identity of the inhibitor used. In SMPs piericidin A gave an FCC of 0.36 for complex I—this value is now consistent with the principles of flux control analysis. In membranes, piericidin A gave FCCs of 0.19 and 0.67 in the absence and presence of exogenous cyt *c*, respectively. These values make sense, because cyt *c* increases the rate of the complex III+IV segment of the chain, rendering complex I more rate-limiting and so increasing its FCC. Finally, using the irreversible

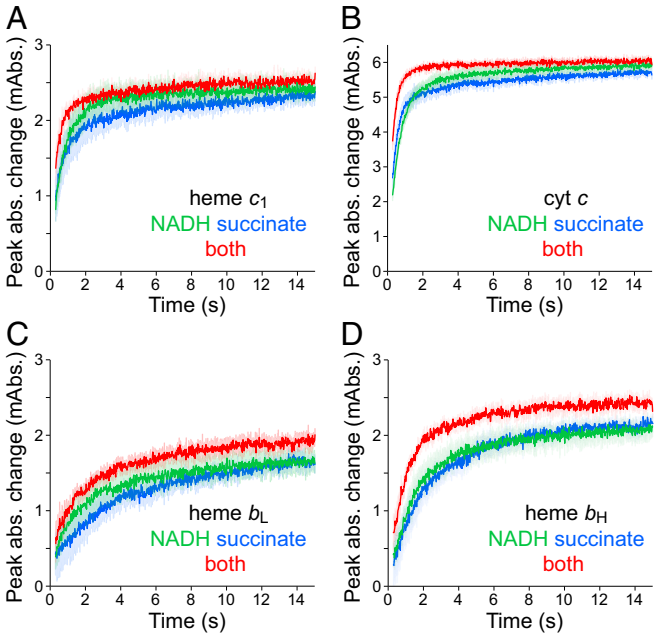

Fig. 3. Reduction of complex III upon addition of NADH, succinate, or both to SMPs. The redox status of the heme centers in complex III and of cyt *c* in SMPs were followed spectroscopically, as described in Fig. 2. (*A*) Heme c_1; (*B*) cyt *c*; (*C*) heme b_L; (*D*) heme b_H. SMPs (500 μg·mL^{-1}, prepared with additional cyt *c*) were reduced anaerobically by addition of 5 mM succinate, 150 μM NADH, or 5 mM succinate and 150 μM NADH together in the presence of 5 μg·mL^{-1} gramicidin. Three technical replicates of each experiment are presented as mean averages ± SEM (n = 3).

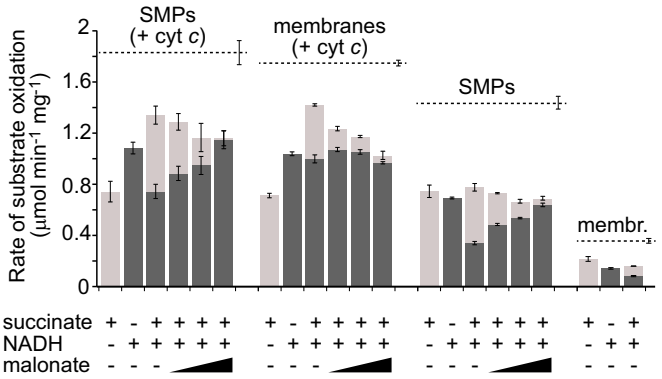

Fig. 4. Comparison of the steady-state rates of individual and simultaneous NADH and succinate oxidation in SMPs and membranes. Light gray, contributions from succinate oxidation; dark gray, contributions from NADH oxidation. The dashed line above each dataset represents the combined individual rates. Values were deduced from simultaneous measurement of the rates of O_2 reduction and NADH oxidation (see *Materials and Methods* for details). Malonate (a competitive complex II inhibitor) was added to 0.145, 0.29, and 7.25 mM; when malonate was added the rates were too low to measure accurately in membranes without additional cyt *c*. Gramicidin (5 μg·mL^{-1}) was included in SMP experiments. Values reported are the mean average of at least three technical replicates and are ± SEM values.

complex I flavin-site inhibitor diphenyleneiodonium (DPI) (25) in SMPs we measured an FCC of 0.42, close to the value measured using piericidin A.

Rotenone FCC values cannot be interpreted within the framework of flux control analysis, and they are clearly different from the values obtained using piericidin A and DPI. Therefore, previously reported rotenone FCC values are not valid as kinetic evidence for substrate channeling. The behavior of rotenone in the flux control analysis can be explained by considering substrate and inhibitor kinetics: In these analyses, catalysis by complex I alone was measured using ubiquinone-1, a hydrophilic quinone substrate present at 100 μM, whereas complex I catalyzing in the overall pathway uses ubiquinone-10, the hydrophobic physiological substrate trapped in the membrane. A reversible, competitive inhibitor will inhibit the two different substrates, which have different binding affinities, to different levels, even when present at a common concentration—this explains the meaningless FCC values observed using rotenone. Conversely, DPI is an irreversible, noncompetitive inhibitor that inhibits to the same extent regardless of the substrate identity or concentration; it provides meaningful FCCs (26). Piericidin A, although known to bind in the ubiquinone-binding site (27), apparently does not behave as a reversible, competitive inhibitor (one that rapidly and repeatedly binds and dissociates on the catalytic timescale, responding to the substrate identity and concentration). Indeed, although not the focus of this work, the ability of this experiment to differentiate the behavior of rotenone and piericidin A provides a new perspective on the large and diverse set of complex I "Q-site" inhibitors.

Discussion

In this work we formulated three conceptually simple predictions for the behavior of the mammalian respiratory chain with outcomes that depend on whether the Q pool in the inner membrane is partitioned into respirasomes (and the substrate is channeled between the enzymes therein) or is simply a freely accessible single pool in the membrane. We found no evidence for partitioning or channeling, and our results indicate the presence of a single pool. Consequently, we revisited the major experimental evidence for Q partitioning and channeling. First, for flux control analysis we found that the FCCs (that underpin the channeling interpretation) depend strongly on the inhibitor used; for a competitive inhibitor the level of inhibition changes according to the Q species involved, and previous analyses using rotenone (15) did not account for this. Alternative inhibitors provide no evidence for substrate channeling. Second, we consider the kinetic evidence reported by Lapuente-Brun et al. (13), using cells with a constitutively low level of complex III. Their observation that decreasing the amount of complex I present increases the complex II activity (but not vice versa) is taken as evidence for substrate channeling within I+III supercomplexes, such that lack of complex I "releases" complex III and makes it available to the complex II pathway. The data shown here in Fig. 4 are a tightly controlled match to this experiment; our data for complexes I and II are equivalent and readily explained by competition of complex I and II for a common Q pool. Alternative nonsupercomplex explanations for the data of Lapuente-Brun et al. (13) include an adaptive increase in complex II, or a decrease in complex II inhibition [decreasing the activity of complex I in mitochondria increases matrix NADH, shifting the balance of malate and oxaloacetate (catalyzed by malate dehydrogenase) toward malate and decreasing the concentration of oxaloacetate, a complex II inhibitor (28)]. We conclude that there is no extant evidence for Q-pool partitioning or Q channeling and thus contend that supercomplex assemblies are not functionally relevant for respiratory-chain catalysis. Our conclusion mirrors that of Trouillard et al. (16), who used time-resolved spectroscopic methods to exclude cyt *c* channeling or partitioning in yeast, and is also in line with a substantial body of earlier work (that predates the blue native PAGE analyses that reinvigorated interest in respiratory-chain organization), including detailed considerations of the diffusion properties of ubiquinone and its pool characteristics (1–3, 29, 30).

Structural analyses of the mammalian I+III$_2$+IV supercomplex by electron microscopy have estimated distances of 130 Å between the Q binding sites of complexes I and III, and 100 Å between the cyt *c* binding sites of complexes III and IV (8, 9). These are substantial distances—for reference, the large hydrophilic domain of complex I extends ~140 Å above the membrane (31). Both sets of authors evaluated their structures for substrate channeling but formed opposing opinions: Dudkina et al. (9) doubt whether the distances support a kinetic justification for supercomplex formation, whereas Althoff et al. (8) consider that the supercomplex provides pathways for efficient transfer. In any case, a "channel" is not simply the shortest route for substrate transfer—it is a route that does not allow exchange with the outside. Illustrative examples are the CO-transferring channel in the CO–dehydrogenase complex, and the carbamate and NH_4^+ tunnels in carbamoyl phosphate synthetase, which contain closed tunnels to lock intermediate substrates inside the complex (32). In both supercomplex structures cyt *c* is clearly visible on the outside of the assembly and the membrane domains of the complexes do not interact directly but are "glued together" by layers of phospholipids; these lipids provide pathways for exchanging Q outside

Table 1. Rates of steady-state catalysis by SMPs for reactions involving complexes I and II

Reaction	Rate, μmol·min^{-1}·mg^{-1}*
NADH:O_2 oxidoreduction†	0.210 ± 0.003
Succinate:NAD^+ oxidoreduction (ATP supported)‡	0.234 ± 0.010
Succinate:O_2 oxidoreduction§	0.354 ± 0.009
NADH:fumarate oxidoreduction¶	0.051 ± 0.002

SMPs were prepared without additional cyt *c*.
*Values reported are the mean average of at least three technical replicates and are ± SEM values.
†Measured using 100 μM NADH.
‡Complex I was activated using 10 μM NADH and then 1 mM ATP, 1 mM $MgSO_4$, and 0.4 mM NaCN were added and the reaction initiated with 10 mM succinate and 1 mM NAD^+.
§10 mM succinate, measured using a Clark electrode.
¶Measured using 200 μM NADH, 1.5 mM fumarate, and 0.4 mM NaCN.

Table 2. Measurement of the flux control coefficients for complexes I and II catalyzing NADH:O_2 and succinate:O_2 oxidoreduction, respectively, by SMPs and mitochondrial membranes

Experimental system	Inhibitor	Slope of inhibition titration*		Flux control coefficient
		O_2 reduction	Q_1 reduction	
SMPs[†] + NADH[‡]	Rotenone	−2.13 ± 0.14	−1.27 ± 0.06	1.68 ± 0.13
	Piericidin A	−1.87 ± 0.29	−5.26 ± 0.33	0.36 ± 0.06
	DPI	−0.69 ± 0.09	−1.64 ± 0.08	0.42 ± 0.06
SMPs[†] + succinate[§]	Atpenin A5	−5.17 ± 0.32	−4.43 ± 0.55	1.17 ± 0.16
Membranes + NADH[‡]	Rotenone	−3.95 ± 0.22	−1.63 ± 0.19[‖]	2.42 ± 0.31
	Piericidin A	−2.30 ± 0.14	−12.15 ± 0.43[‖]	0.19 ± 0.01
Membranes + cyt c[¶] + NADH[‡]	Rotenone	−6.29 ± 0.36	−1.63 ± 0.19[‖]	3.86 ± 0.50
	Piericidin A	−8.20 ± 0.32	−12.15 ± 0.43[‖]	0.67 ± 0.04

*All values are the mean average of at least three technical replicates and are ± SEM values. The units are percent inhibition (nanomolar inhibitor)$^{-1}$, measured at low inhibitor concentrations.
[†]SMPs were prepared without additional cyt *c* and were uncoupled by 10 μg·mL^{-1} gramicidin.
[‡]200 μM NADH, with NADH oxidation measured spectroscopically.
[§]5 mM succinate, with succinate oxidation measured using a coupled assay system.
[¶]1.5 μM cyt *c*.
[‖]The extent of inhibition does not depend on whether additional cyt *c* is present or not; values reported measured with additional cyt *c*.

of the supercomplex. We conclude that structural data on the I+III$_2$+IV supercomplex are consistent with free exchange of both Q and cyt *c*.

Having discarded a substantial kinetic role for supercomplexes in catalysis, we consider alternative possibilities. It is difficult to envisage mechanistically how supercomplexes could exert primary effects on the formation of reactive oxygen species, and only limited circumstantial evidence has been presented to support this proposal (33). Effects on complex stability and assembly (34) have been proposed but support for the stability hypothesis is based on genetic ablation of "partner" enzymes (35–37), causing substantial disruption that impedes respiratory-chain turnover. This decreased turnover causes upstream species such as NADH to accumulate and oxidative stress to increase, thus providing a plausible supercomplex-free explanation of the results (38). Instead, we consider it more likely that supercomplexes influence (or are caused by) the morphology and/or protein-packing density of the mitochondrial inner membrane. The incorporation of ATP synthase dimers into highly curved membrane structures is well known (10), and a relationship between respiratory-chain supercomplexes and membrane topology has recently been proposed (39).

We close by proposing a different explanation for respiratory-chain supercomplex formation within the inner mitochondrial membrane, an extremely densely packed environment with one of the highest protein:lipid ratios in the cell. We propose that supercomplexes have evolved in response to pressure to maintain an extremely high protein concentration but avoid nucleation and aggregation: A set of preferred, weak, and reversible intercomplex interactions preclude the formation of irreversible strong interactions. A similar proposal has been made for αB-crystallin, a major protein of the eye lens, for which weak interactions are speculated to maintain a very high protein concentration but avoid a phase transition (40, 41). Correspondingly, the absence of known supercomplex-mediating factors in extensive structural data on isolated complexes III and IV, the lack of strong contact points in the I+III$_2$+IV supercomplex (8, 9), and the delicate nature of supercomplexes (which rely on very mild detergents for their isolation) are all consistent with weak and transient associations that only become "fixed" when the membrane is partially disrupted.

Materials and Methods

Preparation of Mitochondria, Membranes, and SMPs. Bovine heart mitochondria, membranes, and SMPs were prepared using methods described previously (17, 42) with minor modifications. In some preparations of SMPs (referred to as SMPs with additional cyt *c*) 1 mg·mL^{-1} of equine cyt *c* (Sigma) was incubated with the mitochondria for 1 h before sonication. See *SI Text* for details.

Blue Native PAGE Analyses. Samples (~5 mg protein·mL^{-1}) were solubilized by incubation on ice for 20 min in 1% (wt/vol) digitonin (Calbiochem) and centrifuged, and 50–60 μg protein (per lane) were applied to 3–12% Tris-glycine native-PAGE gels (Invitrogen) and run according to the manufacturer's instructions. Proteins were visualized using colloidal Coomassie R250, or the gel strips were destained with MilliQ water for in-gel assays performed using 150 μM NADH and 1 mg·mL^{-1} nitro blue tetrazolium (NBT) for complex I, or 84 mM succinate, 0.2 mM phenazine methosulfate (PMS), 2 mg·mL^{-1} NBT, and 10 mM NaCN for complex II (18).

Heme Spectroscopy. Spectra were recorded from 491.2 to 649.6 nm in a 200-μL quartz cuvette using a photodiode array with a step of 2.1 nm (Applied Photophysics Ltd.) housed in an anaerobic glovebox (O_2 <10 ppm). Experiments were conducted with 500 μg protein·mL^{-1} SMPs, in 10 mM Tris-SO_4 (pH 7.4) with 250 mM sucrose, at 32 °C, with 5 μg·mL^{-1} gramicidin to dissipate Δp. A reference spectrum was collected before addition of the reductant (5 mM succinate and/or 150 μM NADH), and all spectra were gathered in the reduced-oxidized mode; the time course for heme c_1 reduction was used to align traces and account for variation in the manual mixing zero-time point. Spectra were deconvoluted using Eq. **1**:

$$\mathbf{C} = \mathbf{A}(\mathbf{S}^{\mathrm{T}}\mathbf{S})^{-1}\mathbf{S}^{\mathrm{T}}, \quad [1]$$

where **C** is the unknown column matrix containing the concentration of each component, **A** is the column matrix containing the observed absorbances at each wavelength, and **S** is the known matrix containing the absorbance of each heme center at each wavelength (19, 20). The known spectra of hemes a_L and a_3 were taken from ref. 43, and b_H, b_L, and a_H were from ref. 44; the spectra of cyt *c* and heme c_1 were measured directly.

Combined O_2 Reduction and NADH/Succinate Oxidation Measurements. Measurements were conducted at 32 °C in a 4.5-mL cuvette, sealed with a steel lid fitted with a Clark-type micro-oxygen electrode (ADInstruments) and two small ports for addition of reagents. Spectra, to quantify NADH oxidation [$\varepsilon_{(340-380nm)}$ = 4.81 mM^{-1}·cm^{-1}], were recorded simultaneously with O_2 consumption using a fiber optic Ocean Optics S2000 diode-array spectrometer. All solutions contained 10 mM Tris-SO_4 (pH 7.5), 250 mM sucrose, and 5,000 U·mL^{-1} catalase to increase stability. SMPs (20–40 μg·mL^{-1}) were used with 5 μg·mL^{-1} gramicidin to collapse Δp, 60 μg·mL^{-1} mitochondrial membranes, or 30 μg·mL^{-1} membranes with 1.65 μM cyt *c* (Fig. S4). Reactions were initiated by 150 μM NADH (65 μM for membranes without extra cyt *c*, owing to high solution turbidity) or 5 mM succinate, and subsequent additions of succinate and/or malonate were made with a minimum of 30-s intervals. Control samples were confirmed to maintain a constant rate of catalysis throughout the experimental time scale. Succinate oxidation rates were calculated as the difference between the measured rates of O_2 reduction and NADH oxidation. The O_2 electrode was calibrated using the consumption of known amounts of NADH.

Standard Spectrophotometric Assays. All measurements were made in 10 mM Tris-SO_4 (pH 7.4) and 250 mM sucrose, at 32 °C, using a 96-well Molecular Devices plate reader. NADH oxidation was monitored directly [$\varepsilon_{(340–380nm)}$ = 4.81 $mM^{-1}{\cdot}cm^{-1}$] and succinate oxidation was monitored using a coupled assay system (45). Inhibitor titrations used 50 $\mu g{\cdot}mL^{-1}$ SMPs or membranes, with 10 $\mu g{\cdot}mL^{-1}$ gramicidin added for SMPs and 1.5 μM cyt *c* added for membranes (Fig. S4) when stated. Rotenone (0–500 nM), piericidin A (0–50 nM), and atpenin A5 (0–50 nM) were added from ethanolic stock solutions and incubated for 10 min before addition of substrate. DPI (0–425 nM) was added from a DMSO stock solution and incubated at 4 °C in the presence of 1 mM NADH for 2 h before the experiment (DPI reacts slowly with the reduced flavin). For measurements with ubiquinone-1, 100 μM ubiquinone-1 was added 10 min before the inhibitor, with 0.5 mM NaCN present to inhibit complex IV.

ACKNOWLEDGMENTS. We thank Dr. R. J. Springett [Medical Research Council (MRC)] for heme spectra and Dr. E. Fernández-Vizarra (MRC) for advice on blue native PAGE analyses. This research was funded by MRC Grant U105663141.

1. Kröger A, Klingenberg M (1973) The kinetics of the redox reactions of ubiquinone related to the electron-transport activity in the respiratory chain. *Eur J Biochem* 34(2): 358–368.
2. Gupte S, et al. (1984) Relationship between lateral diffusion, collision frequency, and electron transfer of mitochondrial inner membrane oxidation-reduction components. *Proc Natl Acad Sci USA* 81(9):2606–2610.
3. Chazotte B, Hackenbrock CR (1988) The multicollisional, obstructed, long-range diffusional nature of mitochondrial electron transport. *J Biol Chem* 263(28):14359–14367.
4. Schägger H, Pfeiffer K (2000) Supercomplexes in the respiratory chains of yeast and mammalian mitochondria. *EMBO J* 19(8):1777–1783.
5. Acín-Pérez R, Fernández-Silva P, Peleato ML, Pérez-Martos A, Enriquez JA (2008) Respiratory active mitochondrial supercomplexes. *Mol Cell* 32(4):529–539.
6. Acin-Perez R, Enriquez JA (2014) The function of the respiratory supercomplexes: The plasticity model. *Biochim Biophys Acta* 1837(4):444–450.
7. Schägger H, Pfeiffer K (2001) The ratio of oxidative phosphorylation complexes I-V in bovine heart mitochondria and the composition of respiratory chain supercomplexes. *J Biol Chem* 276(41):37861–37867.
8. Althoff T, Mills DJ, Popot J-L, Kühlbrandt W (2011) Arrangement of electron transport chain components in bovine mitochondrial supercomplex $I_1III_2IV_1$. *EMBO J* 30(22): 4652–4664.
9. Dudkina NV, Kudryashev M, Stahlberg H, Boekema EJ (2011) Interaction of complexes I, III, and IV within the bovine respirasome by single particle cryoelectron tomography. *Proc Natl Acad Sci USA* 108(37):15196–15200.
10. Davies KM, et al. (2011) Macromolecular organization of ATP synthase and complex I in whole mitochondria. *Proc Natl Acad Sci USA* 108(34):14121–14126.
11. Strogolova V, Furness A, Robb-McGrath M, Garlich J, Stuart RA (2012) Rcf1 and Rcf2, members of the hypoxia-induced gene 1 protein family, are critical components of the mitochondrial cytochrome bc_1-cytochrome *c* oxidase supercomplex. *Mol Cell Biol* 32(8):1363–1373.
12. Chen Y-C, et al. (2012) Identification of a protein mediating respiratory supercomplex stability. *Cell Metab* 15(3):348–360.
13. Lapuente-Brun E, et al. (2013) Supercomplex assembly determines electron flux in the mitochondrial electron transport chain. *Science* 340(6140):1567–1570.
14. Ikeda K, Shiba S, Horie-Inoue K, Shimokata K, Inoue S (2013) A stabilizing factor for mitochondrial respiratory supercomplex assembly regulates energy metabolism in muscle. *Nat Commun* 4:2147.
15. Bianchi C, Genova ML, Parenti Castelli G, Lenaz G (2004) The mitochondrial respiratory chain is partially organized in a supercomplex assembly: Kinetic evidence using flux control analysis. *J Biol Chem* 279(35):36562–36569.
16. Trouillard M, Meunier B, Rappaport F (2011) Questioning the functional relevance of mitochondrial supercomplexes by time-resolved analysis of the respiratory chain. *Proc Natl Acad Sci USA* 108(45):E1027–E1034.
17. Pryde KR, Hirst J (2011) Superoxide is produced by the reduced flavin in mitochondrial complex I: A single, unified mechanism that applies during both forward and reverse electron transfer. *J Biol Chem* 286(20):18056–18065.
18. Wittig I, Karas M, Schägger H (2007) High resolution clear native electrophoresis for in-gel functional assays and fluorescence studies of membrane protein complexes. *Mol Cell Proteomics* 6(7):1215–1225.
19. Sternberg JC, Stillo HS, Schwendeman RH (1960) Spectrophotometric analysis of multicomponent systems using least squares method in matrix form. Ergosterol irradiation system. *Anal Chem* 32:84–90.
20. Shinkarev VP, Crofts AR, Wraight CA (2006) Spectral and kinetic resolution of the bc_1 complex components *in situ*: A simple and robust alternative to the traditional difference wavelength approach. *Biochim Biophys Acta* 1757(4):273–283.
21. Iwaki M, et al. (2003) Redox-induced transitions in bovine cytochrome bc_1 complex studied by perfusion-induced ATR-FTIR spectroscopy. *Biochemistry* 42(38):11109–11119.
22. Cecchini G, Schröder I, Gunsalus RP, Maklashina E (2002) Succinate dehydrogenase and fumarate reductase from *Escherichia coli*. *Biochim Biophys Acta* 1553(1–2):140–157.
23. Fell DA (1992) Metabolic control analysis: A survey of its theoretical and experimental development. *Biochem J* 286(Pt 2):313–330.
24. Horsefield R, et al. (2006) Structural and computational analysis of the quinone-binding site of complex II (succinate-ubiquinone oxidoreductase): A mechanism of electron transfer and proton conduction during ubiquinone reduction. *J Biol Chem* 281(11):7309–7316.
25. Majander A, Finel M, Wikström M (1994) Diphenyleneiodonium inhibits reduction of iron-sulfur clusters in the mitochondrial NADH-ubiquinone oxidoreductase (Complex I). *J Biol Chem* 269(33):21037–21042.
26. Moreno-Sánchez R, Saavedra E, Rodríguez-Enríquez S, Olín-Sandoval V (2008) Metabolic control analysis: A tool for designing strategies to manipulate metabolic pathways. *J Biomed Biotechnol* 2008:597913.
27. Baradaran R, Berrisford JM, Minhas GS, Sazanov LA (2013) Crystal structure of the entire respiratory complex I. *Nature* 494(7438):443–448.
28. Kearney EB, Ackrell BAC, Mayr M (1972) Tightly bound oxalacetate and the activation of succinate dehydrogenase. *Biochem Biophys Res Commun* 49(4):1115–1121.
29. Green DE, Tzagoloff A (1966) The mitochondrial electron transfer chain. *Arch Biochem Biophys* 116(1):293–304.
30. Rich PR (1984) Electron and proton transfers through quinones and cytochrome *bc* complexes. *Biochim Biophys Acta* 768(1):53–79.
31. Vinothkumar KR, Zhu J, Hirst J (2014) Architecture of mammalian respiratory complex I. *Nature*, in press.
32. Weeks A, Lund L, Raushel FM (2006) Tunneling of intermediates in enzyme-catalyzed reactions. *Curr Opin Chem Biol* 10(5):465–472.
33. Genova ML, Lenaz G (2014) Functional role of mitochondrial respiratory supercomplexes. *Biochim Biophys Acta* 1837(4):427–443.
34. Moreno-Lastres D, et al. (2012) Mitochondrial complex I plays an essential role in human respirasome assembly. *Cell Metab* 15(3):324–335.
35. Schägger H, et al. (2004) Significance of respirasomes for the assembly/stability of human respiratory chain complex I. *J Biol Chem* 279(35):36349–36353.
36. Acín-Pérez R, et al. (2004) Respiratory complex III is required to maintain complex I in mammalian mitochondria. *Mol Cell* 13(6):805–815.
37. Diaz F, Fukui H, Garcia S, Moraes CT (2006) Cytochrome *c* oxidase is required for the assembly/stability of respiratory complex I in mouse fibroblasts. *Mol Cell Biol* 26(13): 4872–4881.
38. Diaz F, Enríquez JA, Moraes CT (2012) Cells lacking Rieske iron-sulfur protein have a reactive oxygen species-associated decrease in respiratory complexes I and IV. *Mol Cell Biol* 32(2):415–429.
39. Cogliati S, et al. (2013) Mitochondrial cristae shape determines respiratory chain supercomplexes assembly and respiratory efficiency. *Cell* 155(1):160–171.
40. Jehle S, et al. (2011) N-terminal domain of αB-crystallin provides a conformational switch for multimerization and structural heterogeneity. *Proc Natl Acad Sci USA* 108(16):6409–6414.
41. Slingsby C, Wistow GJ, Clark AR (2013) Evolution of crystallins for a role in the vertebrate eye lens. *Protein Sci* 22(4):367–380.
42. Walker JE, Skehel JM, Buchanan SK (1995) Structural analysis of NADH:ubiquinone oxidoreductase from bovine heart mitochondria. *Methods Enzymol* 260:14–34.
43. Liao GL, Palmer G (1996) The reduced minus oxidized difference spectra of cytochromes *a* and a_3. *Biochim Biophys Acta* 1274(3):109–111.
44. Kim N, Ripple MO, Springett R (2011) Spectral components of the α-band of cytochrome oxidase. *Biochim Biophys Acta* 1807(7):779–787.
45. Jones AJY, Hirst J (2013) A spectrophotometric coupled enzyme assay to measure the activity of succinate dehydrogenase. *Anal Biochem* 442(1):19–23.